

Available online at [www.sciencedirect.com](http://www.sciencedirect.com)

ScienceDirect

journal homepage: [www.elsevier.com/locate/AJPS](http://www.elsevier.com/locate/AJPS)

## Original Research Paper

# Changes in target ability of nanoparticles due to protein corona composition and disease state

Wenwen Xu<sup>a</sup>, Mingyu Xu<sup>a</sup>, Yumeng Xiao<sup>a</sup>, Lu Yu<sup>b</sup>, Huiru Xie<sup>b</sup>, Xuehua Jiang<sup>a</sup>,  
Meiwan Chen<sup>c</sup>, Huile Gao<sup>a,\*</sup>, Ling Wang<sup>a,\*</sup>

<sup>a</sup> Key Laboratory of Drug-Targeting and Drug Delivery System of the Education Ministry, Sichuan Engineering Laboratory for Plant-Sourced Drug and Sichuan Research Center for Drug Precision Industrial Technology, West China School of Pharmacy, Sichuan University, Chengdu 610064, China

<sup>b</sup> Chengdu Finelyse Pharmaceutical Technology Co. Ltd, Chengdu 610064, China

<sup>c</sup> State Key Laboratory of Quality Research in Chinese Medicine, Institute of Chinese Medical Sciences, University of Macau, Macau, China

## ARTICLE INFO

## Article history:

Received 3 December 2021

Revised 14 January 2022

Accepted 4 March 2022

Available online 4 April 2022

## Keywords:

Protein corona

Diabetes mellitus

Comorbidity

Targeting capability

## ABSTRACT

Many studies have shown the influence of protein corona (PC) on the active targeting capability of ligand-modified nanoparticles; however, the influence of clinical status on PC composition and targeting capacity is rarely discussed. In this study, when transferrin-modified PEGylated polystyrene nanoparticles (Tf-PNs) is intravenously injected into mice with non-small cell lung cancer (NSCLC) comorbid with type 2 diabetes mellitus (T2DM), more Tf-PNs accumulated in the tumor tissue than in those of NSCLC model mice. This indicated that PC derived from different states of disease changed the active targeting ability of Tf-PNs. To explain the occurrence of this phenomenon, our analysis of PC from different disease states revealed that Tf (transferrin) modification had no significant effect on the formation of PC, and that the PC from the NSCLC comorbid with T2DM model contained more proteins like fibrin and clusterin. This work demonstrates the impacts of comorbidity, such as with T2DM, on the active targeting capability of ligand-modified nanoparticles, and the results promote the application of nanoparticles for precision medicine.

© 2022 Shenyang Pharmaceutical University. Published by Elsevier B.V.

This is an open access article under the CC BY-NC-ND license

(<http://creativecommons.org/licenses/by-nc-nd/4.0/>)

## 1. Introduction

Engineered nanoparticles have been considered a powerful and promising tool for drug delivery, but few of them have been approved for clinical application [1,2]. There

remains a wide gap between laboratory discovery and clinical translation, mainly because of the inevitable surface biotransformation of nanoparticles [3]. When exposed to biological environments, nanoparticles non-selectively absorb to various biomolecules, forming a protein corona (PC). The formation of PC can significantly change nanoparticle

\* Corresponding authors.

E-mail addresses: [gaohuile@scu.edu.cn](mailto:gaohuile@scu.edu.cn) (H.L. Gao), [wlin\\_scu@scu.edu.cn](mailto:wlin_scu@scu.edu.cn) (L. Wang).

Peer review under responsibility of Shenyang Pharmaceutical University.

properties, such as size, surface chemistry, and charge [4,5]. PC can alter the nanoparticle's toxicological, pharmacokinetic, and pharmacological profile, including circulation time, tissue distribution, cellular recognition, and even intracellular distribution [6–8]. Therefore, it is of great significance to evaluate the formation of PC in biological conditions and its impact on the performance of nanoparticulate drug delivery systems.

Target nanomedicines have been illustrated in practice, and meet varying levels of success by exploiting specific ligands on the surface of nanoparticles [9,10]. Though possible in theory and *in vitro* experiments, they are not feasible in clinical practice [3]. Recent studies have shown that PC might have a significant influence on the targeting ability of nanomedicines. PC may cause a loss in target ability by masking the targeting ligands [11,12]. However, the attached PC may contain some specific proteins that help nanoparticles be retargeted [9,13–15]. The proteins could attach to the surface of nanoparticles or penetrate the gap of the targeting ligand, thereby changing the targeting efficiency and making the targeting result unpredictable.

The composition of PC largely depends on the protein components in human plasma. Additionally, the type of disease plays a vital role in the protein composition of PC. Some research indicates that the PC attached to nanoparticles is significantly different in patients with cancer, diabetes, pregnancy, and hemophilia A, compared to healthy subjects [16–18]. Due to differences in plasma protein composition in different disease states, proteins adsorbed to nanoparticles may be different, thus affecting the function of nanomaterials. Studies have shown that albumin and apolipoprotein-enriched PC on the surface of nanoparticles may reduce the uptake in immune cells (monocytes, dendritic cells, and macrophages) [19,20]. On the contrary, opsonin-enriched PC might induce the uptake of nanoparticles by macrophages and be quickly cleared out of the body [21]. An in-depth study of how disease states affect targeted nanoparticles and what function the proteins perform can help us find a way to improve the targeting ability of nanoparticles. However, there are many complications that can lead to changes in plasma protein in clinical settings. The impact of underlying comorbidity on PC composition and the targeting of the nanoparticle-PC complex remains unclear. Therefore, this study aims to better understand the effect of the biological environment on nanomaterials.

Non-small cell lung cancer (NSCLC) patients diagnosed comorbid with diabetes have high incidence and mortality [22,23]. Moreover, many studies demonstrated that preexisting diabetes has a significant and adverse influence on the overall survival (OS) of patients with NSCLC [24–27]. PEGylated polystyrene nanoparticles (PEG-PNs) are widely used to evaluate the influence of PC. Transferrin is widely used as a model ligand because the Tf receptor (TfR) is highly expressed in a variety of malignant tumor cells, such as NSCLC and glioma [28,29]. For this reason, we chose NSCLC comorbid with T2DM as a representative of disease, and Tf modified PEG-PNs (Tf-PNs) were selected to evaluate the effect of complication.

We recently proved that NSCLC patient-derived PC diminished the A549 uptake of Tf-PNs in a large part than PC

from healthy volunteers [22]. However, the PC derived from patients with T2DM comorbid with NSCLC differ from those from NSCLC patients. Thus, the PC might have different effects on the biological behavior of nanoparticles. In this study, we incubated PEG-PNs and Tf-PNs with the plasma of NSCLC patients and NSCLC comorbid with T2DM patients to acquire PC-coated PEG-PNs and PC-coated Tf-PNs *in vitro*. Similarly, the *in vivo* PC-coated nanoparticles were established by intravenous injecting nanoparticles into mice intravenously bearing NSCLC or NSCLC comorbid with T2DM. Subsequently, the *in vivo* and *in vitro* behavioral changes in PC-coated PEG-PNs and Tf-PNs were observed through immunofluorescence and live imaging. In addition, the composition of PC was analyzed via proteomics. The results reveal that underlying comorbidity would induce changes in the PC component of nanoparticles and affect the targeting ability of nanoparticles. Our goal is to realize the use of nanoparticles in clinical settings and improve the applicability of precision nanomedicine.

---

## 2. Materials and methods

### 2.1. Human specimens and ethics statement

All human plasma samples were collected at People's Hospital of Xishuangbanna. Plasma samples were isolated by centrifugation from heparinized venous blood obtained from NSCLC patients comorbid with T2DM ( $n = 3$ ) and NSCLC patients ( $n = 3$ ) treated without radio- or chemotherapy. Plasma was stored at  $-80^{\circ}\text{C}$  until use. Informed consent was obtained from each participant before analysis, and the study was approved by the 111 Project (B18035). This study was conducted according to the principles of the Declaration of Helsinki and approved by the Medical Ethics Committee of Sichuan University (K2020005).

### 2.2. Synthesis of fluorescent polystyrene nanoparticles

Fluorescent (coumarin-6 or DiD) labeled polystyrene nanoparticles were synthesized by microemulsion polymerization, and PEG and Tf modification was conducted to synthesize PEGylated polystyrene nanoparticles (PEG-PNs) and Tf modified PEG-PNs (Tf-PNs), as reported previously [4]. A mixture of styrene, 2,2'-azobis (2-methylbutyronitrile) (V59) as an initiator, hexadecane as a hydrophobe, and coumarin-6 as fluorescence marker was added to the aqueous phase containing C16-C18 fatty alcohol ethoxylates (Lutensol AT 50) as a non-ionic surface-active agent and 2-aminoethyl methacrylate hydrochloride as the amino monomer. PEG-PNs were synthesized by the chemical reaction between the amino group on PNs and the NHS end of PEG. Transferrin-modified PEG-PNs was conducted to synthesize Tf-PNs by reacting with the maleimide group (Mal) on PEG [30]. The product was lyophilized to determine the concentration of PNs solution. The size and electric potential of PN was measured by dynamic light scattering (DLS) with NanoZS90 (Malvern Instruments Ltd., Malvern, UK).

### 2.3. Preparation of PC-coated PNs derived from human plasma *in vitro* and mouse plasma *in vivo*

PC-coated PNs derived from human plasma were obtained with PEG-PNs or Tf-PNs (100  $\mu$ l of 50 mg/ml) cultured with 900  $\mu$ l of human plasma (100%, from the comorbidity or NSCLC group) at 37 °C on a shaker away from light for 1 h. For the PC-coated PNs derived from mouse plasma *in vivo*, PNs (100  $\mu$ l, 50 mg/ml) were injected intravenously to C57BL/6 mice. After 10 min, blood was collected and centrifuged at 8000 rpm and 4 °C for 10 min. All the supernatants (plasma with PNs) were combined and loaded onto a Sepharose CL-4B column (16  $\times$  1.0 cm<sup>2</sup>) (Merck KGaA, Darmstadt, Germany). PNs were eluted with PBS and concentrated by ultrafiltration (Amicom Ultra 100KDa, Merck KGaA, Darmstadt, Germany). The concentration of PNs was calculated according to the turbidimetry. The concentration of protein adsorbed to the PN surface was measured with a BCA protein assay kit.

### 2.4. Fluorescence confocal imaging

For fluorescence confocal imaging, A549 (human lung carcinoma epithelial cells) and LLC (mouse Lewis lung carcinoma cells) cells were seeded on coverslips in 12-well plates at a density of 5  $\times$  10<sup>3</sup> cells/well for 24 h of culture expansion. Cells were treated with different coumarin-stained PNs (with/without PC) diluted with serum-free DMEM to an equal concentration (30  $\mu$ g/ml) for 0.5, 1 and 2 h, respectively. Then, cells were washed with PBS and fixed with 4% paraformaldehyde. The nuclei were stained with mounting medium and DAPI (Solarbio, Beijing, China). The fluorescence of coumarin within cells was visualized by laser scanning microscopy (Zeiss LSM, Carl Zeiss AG, Oberkochen, Germany).

### 2.5. Flow cytometry

A549 and LLC cells were seeded, respectively, in 12-well plates at a density of 1  $\times$  10<sup>4</sup> cells/well for 24 h of culture expansion, then treated with different coumarin-stained PNs (with/without PC) diluted with serum-free DMEM to an equal concentration (30  $\mu$ g/ml) for 0.5, 1 and 2 h, respectively. The cells were washed with PBS, detached from the plate with trypsin, collected by centrifugation (1500 rpm, 3 min), resuspended with 150  $\mu$ l PBS, and analyzed by flow cytometry (BD Biosciences Co., Ltd., NJ, USA).

### 2.6. In vivo distribution

In the comorbidity group, adult male C57/BL6 mice were fed a high-fat diet for eight weeks before intraperitoneal injection of streptozotocin (STZ) 50 mg/kg per day for five consecutive days. After injection, a high-fat diet was continued for one week. T2DM mice models were generated successfully if the fasting blood glucose  $\geq$  11.1 mmol/l [31]. Mice of all groups were anesthetized and injected subcutaneously with LLC cells (5  $\times$  10<sup>6</sup>, in 100  $\mu$ l PBS). Mice were subjected to imaging studies when tumor size reached around 100 mm<sup>3</sup>. Tf-PNs and PEG-PNs were freshly prepared and stained with DiD. Tumor-bearing mice were monitored with an IVIS Spectrum

(Perkin Elmer, Inc., Waltham, MA, USA) after tail vein injection of different DiD-loaded PNs (with/without PC; 50 mg/ml, 100  $\mu$ l). Images were captured at 1, 2, 4, 8 and 24 h post-injection. The hearts, livers, spleens, lungs, kidneys, brains, and tumors from all groups were harvested and subjected to fluorescence imaging immediately after fixation in 4% paraformaldehyde.

### 2.7. Proteomics (LC-MS analysis)

The PC of PNs was characterized by label-free proteomic analysis using nano-liquid chromatography-tandem mass spectrometry (carried out at OE Biotech Ltd., Shanghai, China).

### 2.8. Statistical analysis

All data are shown as the mean  $\pm$  SD. All statistical analyses were performed with SPSS 25.0. All figures were performed by GraphPad Prism 9.0, and bioinformatics analysis was performed using the OmicStudio tools at <https://www.omicstudio.cn/tool>. Student's t-test was used to calculate statistical significances.  $P < 0.05$  was considered statistically significant. All experiments were performed in triplicate.

### 2.9. Data availability

The data supporting the findings of this study are available within the paper and the Supplementary Information. All other data are available from the authors upon reasonable request.

---

## 3. Results and discussion

### 3.1. Preparation and characterization of PEG-PNs and Tf-PNs

Tf-PNs and PEG-PNs were synthesized as reported [4,30]. The sizes of the PEG-PNs and Tf-PNs were 94.28  $\pm$  1.10 nm and 104.83  $\pm$  2.95 nm (Supplementary Table S1 and Fig. 2A), respectively. Both had a small polydispersity index (PDI) (Supplementary Table S1 and Fig. 2A), which is consistent with TEM analysis and the round shape of the nanoparticles (Supplementary Table S1 and Fig. 2C). The surface charge of the PEG-PNs and Tf-PNs was 1.04  $\pm$  0.31 mV and 0.67  $\pm$  0.13 mV (Supplementary Table S1 and Fig. 2B), respectively. The similar size and charge might eliminate the effects of physicochemical properties of nanoparticles on protein adsorption and corona composition [32–34].

### 3.2. The effect of disease state on PEG-PNs and Tf-PNs *in vivo* behavior

DiD-loaded PEG-PNs and Tf-PNs were synthesized and administrated intravenously into NSCLC mice and NSCLC comorbid with T2DM mice to reveal the *in vivo* behavior of PNs by fluorescence imaging. PNs accumulated in the tumor tissue at 1 h post-injection and remained in the tumor area for 24 h (Fig. 1A). Organs were harvested 24 h post-injection and visualized by fluorescent imaging (Fig. 1B). This indicated

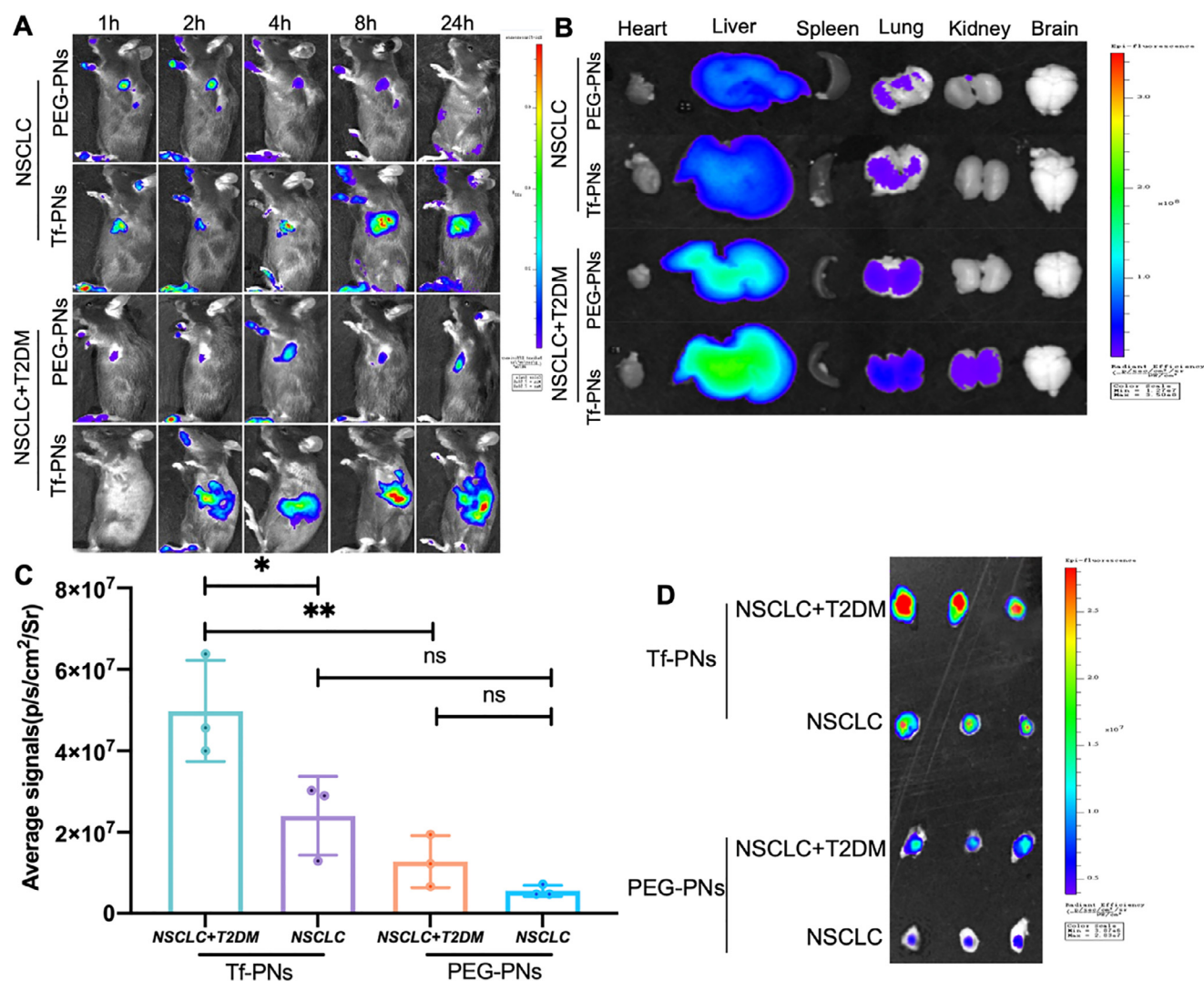


**Fig 1** – *In vivo* distribution of PEG-PNs and Tf-PNs in NSCLC comorbid with T2DM mice or NSCLC mice. (A) Fluorescent images were captured at 1, 2, 4, 8 and 24 h after intravenous injection of PEG-PNs or Tf-PNs in different disease states. (B) Organs and tumors were imaged by fluorescent microscope at 24 h. (D) Fluorescent images of tumors at 24 h, and (C) fluorescence intensity. \*  $P < 0.05$  and \*\*  $P < 0.01$ .

that PNs were mainly captured, metabolized, and cleared by the liver because of the stronger signal in the liver. Among the four groups, Tf-PNs accumulated more in the tumor area than PEG-PNs, and more in the NSCLC comorbid with T2DM group than the NSCLC group (Fig. 1C and 1D). This result shows that the same nanoparticles had different bio-distributions in different disease states, and Tf-PNs accumulated much more in the NSCLC comorbid with T2DM groups.

In conclusion, the state of the disease affects the distribution of nanoparticles. The interaction of receptor on cell and ligand on the nanoparticle surface involved the biological fate of nanoparticles. As is known that proteins in circulation will interact with nanoparticles once injected *in vivo* and form PC on the nanoparticle surface. Thus, we identified the composition of the PC on the nanoparticles and analyzed the difference caused by composition of plasma protein in different disease states.

### 3.3. Characterization of PC-coated PNs *in vivo* and *in vitro*

The different biodistribution of Tf-PNs and PEG-PNs in different disease states may be caused by different PC. We collected and concentrated PNs-coated with PC derived from human plasma *in vitro* and mice plasma *in vivo* to reveal the surface characteristics of the PC. The PN size increased to about 30 nm after forming PC, while the size of all groups was under 150 nm (Fig. 2A). The size of PNs coated with PC derived from human plasma *in vitro* was slightly bigger than that delivered from mice plasma *in vivo*. TEM imaging revealed that PNs retained their spherical structure after being coated PC, even as the size increased (Fig. 2C). Moreover, a layer of vesicular structures surrounding the PN surface was observed, which confirmed the formation of PC. Furthermore, the  $\zeta$ -potential reversed from positive to negative after PC formation

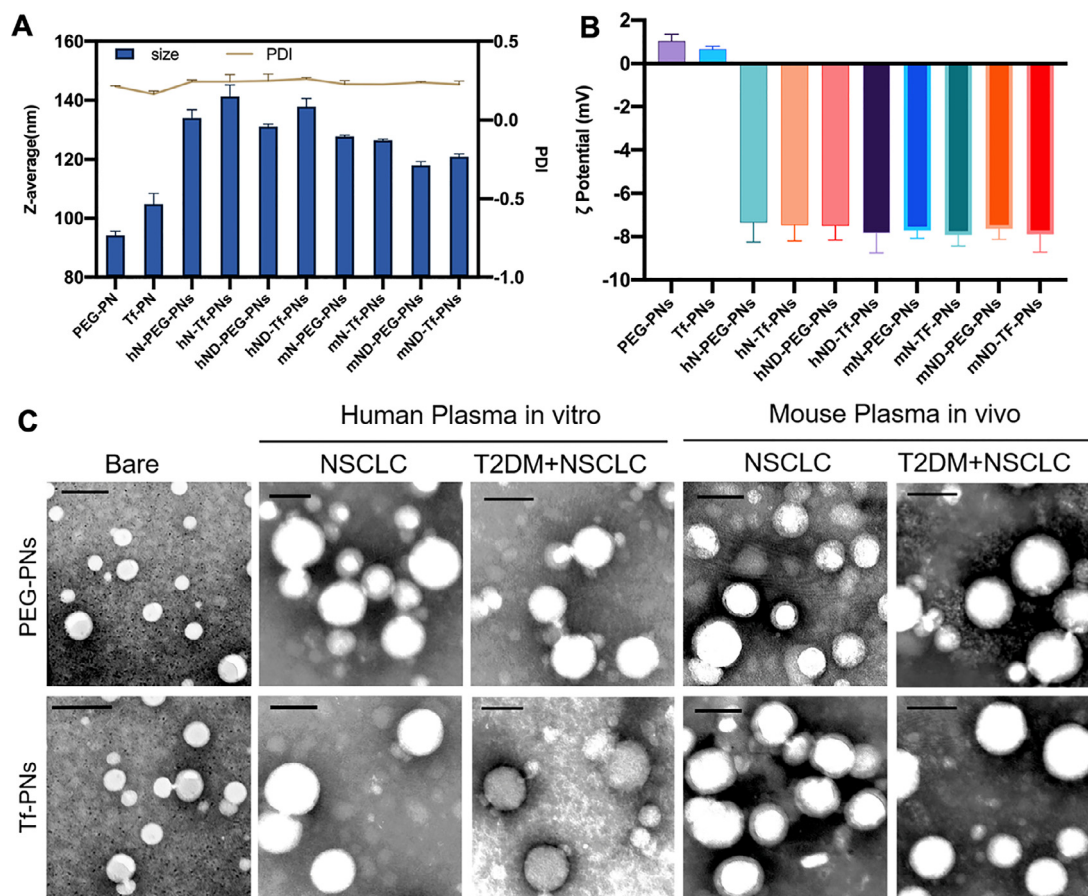


**Fig 2 – Preparation and characterization of PC-coated PNs derived from NSCLC and NSCLC comorbid with T2DM in vivo and in vitro. (A) The Z-average size (nm), PDI and (B) the  $\zeta$ -potential distribution of bare PNs and PC-coated PNs, as determined by DLS. (C) TEM images of PNs and PC-coated PNs. All scale bars are 100 nm.**

(Fig. 2B). In conclusion, the surface properties of the prepared PC-coated Tf-PN and PEG-PN changed considerably.

### 3.4. The effect of human and mice-derived PC on cellular uptake

Bare PNs (PEG-PNs and Tf-PNs), PNs coated with NSCLC human plasma-derived PC (hN-PEG-PNs, hN-Tf-PNs), and PNs coated with NSCLC comorbid with T2DM human plasma-derived PC (hND-PEG-PNs and hND-Tf-PNs) were incubated with A549 cells for a certain time to explore the impact of PC on cellular uptake. The result shows that PNs accumulated in A549 cells in a time-dependent manner. The results showed that A549 cells had higher uptake of Tf-PNs than PEG-PNs in 1 h and 2 h ( $P < 0.01$ ) (Figs. 3A), which indicated that the Tf modification enhanced cellular uptake. Then, A549 cells were exposed to free Tf (500  $\mu$ M) for 1 h before administration of PNs to competitively inhibit the action of the TfR. The result shows that free Tf can considerably decrease the cellular uptake of Tf-PNs ( $P < 0.05$ ), indicating that A549 cells mainly took up Tf-PNs via the TfR-mediated endocytosis pathway (Fig. 3B and 3C).

The accumulation of PNs in A549 cells remarkably decreased, and in both morbid state groups, the difference between PEG-PNs and Tf-PNs disappeared after coating with

PC (Fig. 3A and 3C). This might indicate that the formation of PC impedes nanoparticles entering cells and leads to the loss of target specificity of Tf-PNs. However, the accumulation of all PC-coated PNs in cells was the same, with or without free Tf pre-incubation. This phenomenon indicates that the specific endocytosis of Tf-PNs triggered by TfR disappeared after PC-coating, and that its transportation into the cell also changed after PC-coating. These results are consistent with previous reports that PC may partially or entirely block the ligand, leading to a loss in targeting ability [4,34,35].

In addition, we observed that Tf-PNs with PC derived from NSCLC comorbid with T2DM accumulated more in A549 cells, when compared with that derived from NSCLC patients (Fig. 3A). This difference does not correspond with the change in size and surface charge, but is instead more related to the type and composition of PC protein. Then, the same experiment was performed using LLC cells, which were derived from mice with NSCLC, to verify the cell uptake results of PC derived from mice with NSCLC or mice with NSCLC and T2DM. The cellular uptake of NSCLC mice-derived PNs (mN-PEG-PNs and mN-Tf-PNs) and NSCLC comorbid with T2DM mice-derived PNs (mND-PEG-PNs and mND-Tf-PNs) on LLC cells was similar to that with human derived PC (Figs. 3D and 3E).

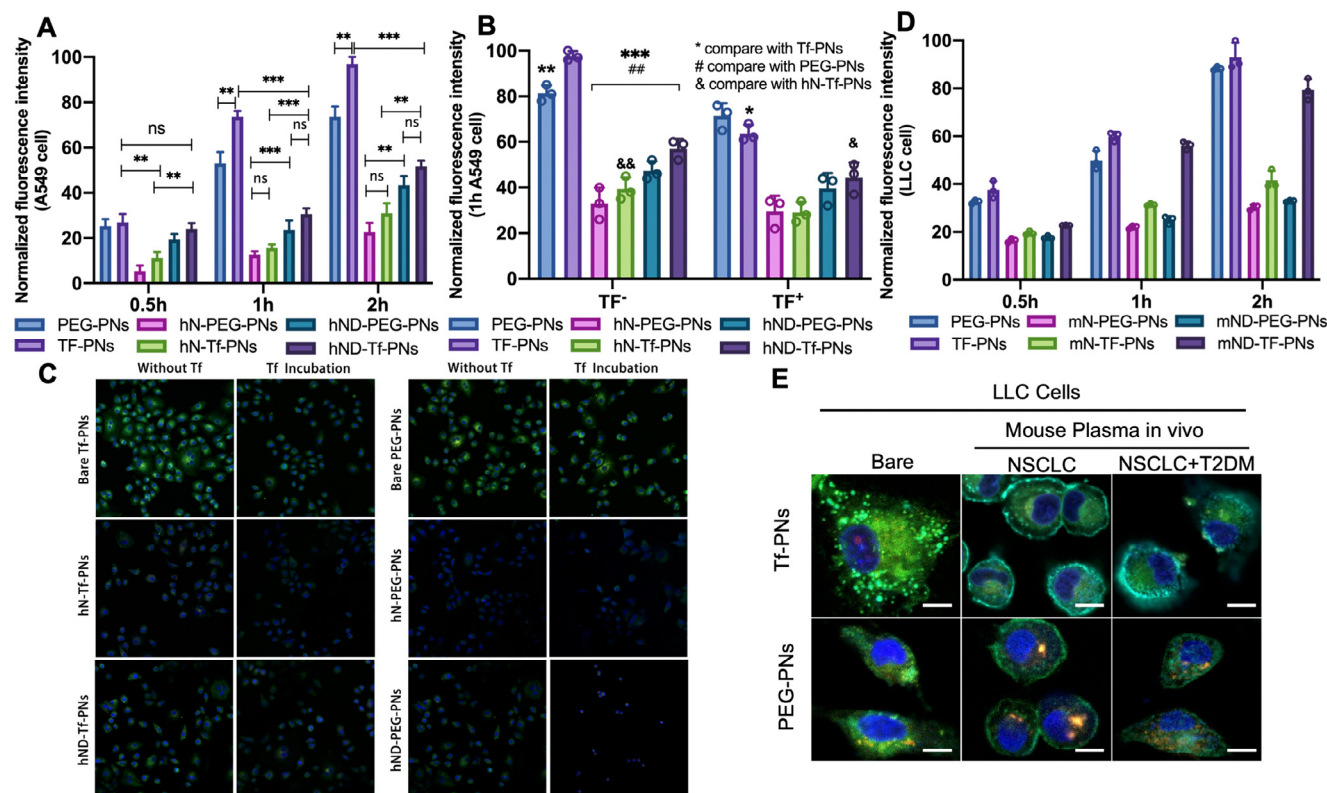


**Fig 3 – Cellular uptake of bare PNs and PC-coated PNs from human plasma *in vitro* and mice plasma *in vivo*.** (A) Accumulation of PNs in A549 cells determined by flow cytometry ( $n = 3$ ). \*\* means  $P < 0.01$ , \*\*\* means  $P < 0.001$  (B) Cellular uptake of PNs in A549 cells for 1 h with and without free Tf in the medium. \* means  $P < 0.05$  and \*\* means  $P < 0.01$  compared with Tf-PNs without Tf incubation, ## means  $P < 0.01$  compared with PEG-PNs without Tf incubation, and & means  $P < 0.01$  compared with hND-Tf-PNs without Tf incubation. (C) Confocal laser scanning microscope images of A549 cells taking up coumarin-stained PNs with and without free Tf in medium. Blue color represented cell nucleus; green represented PNs; red represented lysosomes; scale bar represented  $10 \mu\text{m}$ . (D) Accumulation of PNs in LLC cells with flow cytometry ( $n = 3$ ). (E) Confocal laser scanning microscope images of LLC cells taking up coumarin-stained PNs.

**Table 1 – Protein bound to PNs' coronas. Micrograms of protein per milligram of PNs ( $\mu\text{g}/\text{mg}$ ).**

Groups	Mice-derived PC		Human-derived PC	
	PEG-PNs	Tf-PNs	PEG-PNs	Tf-PNs
NSCLC group	480.93 $\pm$ 6.13	536.67 $\pm$ 32.82	2030.70 $\pm$ 124.81	2394.14 $\pm$ 94.31
Comorbidity group	511.80 $\pm$ 55.61	535.74 $\pm$ 37.71	2179.49 $\pm$ 152.78	2461.34 $\pm$ 90.39

### 3.5. Quantitative analysis of PC derived from human *in vitro* and mice *in vivo*

To explore the difference in PC, the qualitative and quantitative characterization of proteins in them was conducted. Protein-absorbing ability was determined from the mass of protein per mg of PNs absorbed. The amount of protein in each group is presented in Table 1. The Tf-PN absorbed more protein than PEG-PN, which may be due to the ligand modification [36]. Although Tf-PNs could absorb more protein when injected into NSCLC comorbid with T2DM mice, the results showed no statistically significant differences.

The distinct proteomic fingerprints were obtained to reveal the composition of PC by LC/MS. All proteins were displayed and analyzed by relative protein abundance (RPA). First, the protein was categorized according to molecular weight (MW), with 10 kDa as the unit. According to the qualitative results of SDS-page and the quantitative results of proteomics, the largest MW protein was around 20–80 kDa (Figs. S4&S5 and Fig. 4A and 4C). The results indicated that there was no significant difference in the protein MW composition of the PC absorbed by PEG-PNs and Tf-PNs for human plasma *in vitro* or mice plasma *in vivo*. PEG-PNs and Tf-PNs are hydrophilic materials, and they have been reported to mainly absorb

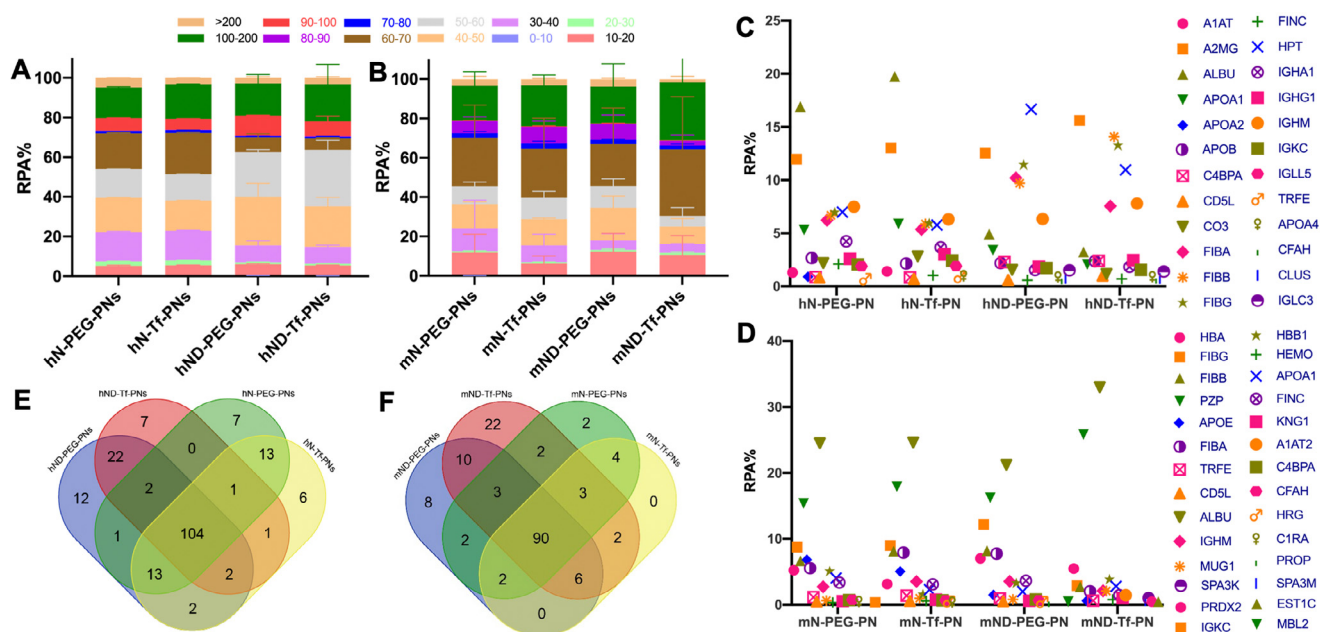


**Fig 4 – Quantitative analysis of PC derived from human plasma and mice plasma. (A) and (B) Relative protein abundance (RPA) of PC identified on PNs by LC-MS recovered from patient plasma and mice plasma, respectively, categorized with 10 kDa as the unit. (C) and (D) The 20 most abundant proteins for each human-derived group and mice-derived group, respectively; (E) and (F) the overlapping and specific proteins of each group treated with nanoparticles derived from human and mice respectively, as showed with Venn diagram.**

albumin, fibrinogen, and IgG [37]. In addition, the PC derived from the NSCLC comorbid with T2DM patients contained more 40–60 kDa proteins and fewer 10–30 kDa proteins.

The 20 most abundant proteins from each human-derived group are displayed in Supplementary Table S2, and those from the mice-derived group are shown in Supplementary Table S4. The abundant proteins likely drive cell interactions, which comprise around 90% of the PC for each nanoparticle. In the results of human blood incubation *in vitro*, there was no significant effect on the type and proportion of adsorbed abundant proteins, with or without Tf modification of the nanoparticles (Fig. 4C). However, the disease state significantly affected the abundant proteins adsorbed on the nanoparticles. Compared with NSCLC patients, Tf-PNs in comorbid patients absorbed more CLUS (clusterin) and CFAH proteins, as well as more coagulation proteins (HPT, C4BPA, FIBB, FIBA and FIBG) related to wound healing and tissue repair [38,39]. However, TRFE, A1AT, ALBU, CO3, FINC, APOA1, and IGHA1 had less absorption. CLUS is a high-density lipoprotein present in plasma. It can be adsorbed to the surface of hydrophilic nanoparticles by hydrogen bonds, thereby increasing the hydrophobicity of nanoparticles and reducing the adsorption of ALBU (serum albumin) [40–42]. Moreover, the accumulation of clusterin in PC could reduce the nonspecific cell uptake by macrophages [43]. The results also show that both Tf-PNs and PEG-PNs absorbed less TRFE (transferrin) in the NSCLC comorbid with T2DM patient plasma (less than 0.5%). Studies have shown that the expression of transferrin is reduced in many cancers, and low levels of transferrin are prognostic biomarkers associated with poor clinical outcomes [44–47].

The Venn diagram shows that 104 proteins were shared among all groups. In addition, hND-Tf-PNs, hND-PEG-PNs, hN-Tf-PNs and hN-PEG-PNs groups contained 7, 12, 6, and 7 types of unique proteins, respectively (Fig. 4E). The same analysis was conducted for mice derived PC *in vivo*. The Venn diagram shows that most proteins (90 proteins) were shared among all groups, and each group contained several unique proteins (Fig. 4F). These results indicate that the different disease statuses of each group contributed to a specific PC composition.

In conclusion, Tf modification had no significant effect on the number and type of protein in the PC. However, the disease status contributes significantly to PC composition, and human NSCLC comorbid with T2DM derived PC contained more fibrin and clusterin, which may help nanoparticles escape non-characteristic intake and increase blood circulation time.

### 3.6. Qualitative analysis of PC derived from human *in vitro*

A qualitative analysis of differential protein of PCs derived from different human disease states was also conducted. The total RPA% of all groups is shown in the heat map (Fig. 5A). PCA analysis demonstrated that the difference between the four groups was statistically significant ( $P < 0.05$ ) (Fig. 5B). The results show a significant difference in the composition of PC derived from plasma of NSCLC comorbid with T2DM patients and NSCLC patients. In classifying proteins by biological function according to uniprot.com (Fig. 5C), the RPA% of coagulation and acute phase proteins was higher in the NSCLC comorbid with T2DM patient group than the NSCLC

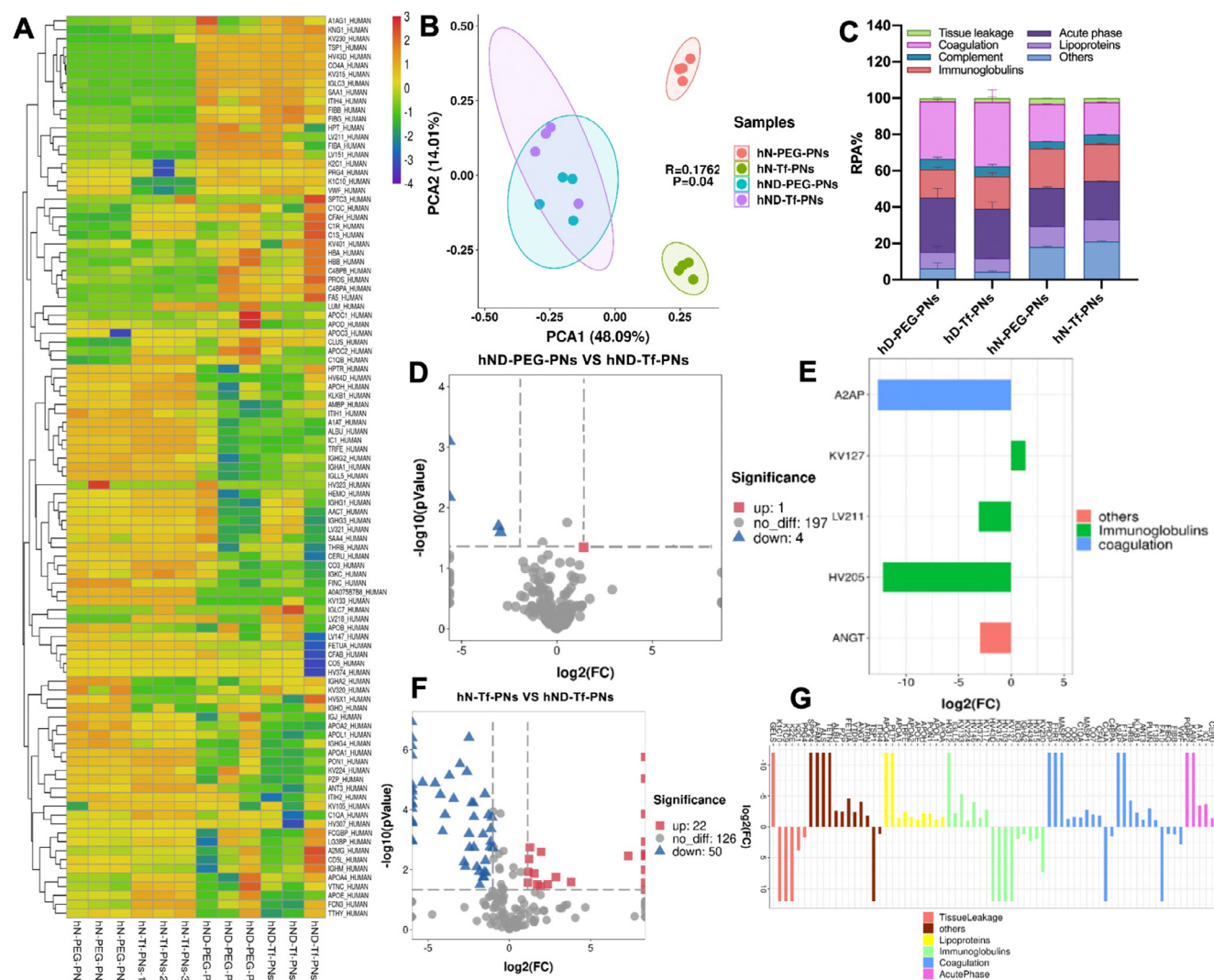


**Fig 5 – Qualitative analysis of PC derived from human plasma *in vitro*. (A) Heat map of RPA% of PC derived from patients. (B) Principal component analysis (PCA) of the corona proteins identified on PNs. (C) Bioinformatic classification of corona proteins. (D) Volcano plot of differential proteins between hND-Tf-PNs and hND-PEG-PNs. The x-axis represents the fold change of proteins, and the dotted line indicates  $FC > 2$  or  $< -2$ . The y-axis represents P value, and the dotted line represents  $P > 0.05$ . (E) Clustering of differential proteins between hND-Tf-PNs and hND-PEG-PNs. (F) Volcano plot of differential proteins between hND-Tf-PNs and hN-Tf-PNs. (G) Clustering of differential proteins between hND-Tf-PNs and hN-Tf-PNs.**

patient group, while the abundances of immunoglobulins and lipoprotein group were lower. Moreover, Tf-PNs absorbed a similar amount of proteins with biological functions in the comorbid group and NSCLC group, which suggests the Tf-modification made no difference in protein adsorption.

A volcano plot was constructed to identify significant differential protein between the two groups, defined at the  $P < 0.05$  level with a fold change of  $> 2$  or  $< -2$ . The volcano plot shows that Tf-PNs and PEG-PNs incubated with the same comorbid plasma had few significant differential proteins in PC (Fig. 5D). Compared with hND-PEG-PNs, there were only five significant differential proteins in hND-Tf-PNs (Fig. 5E) with low content (RPA  $< 0.048\%$ ). Compared with hN-Tf-PNs, there were 72 significant differential proteins in PC of hND-Tf-PNs (Fig. 5F and 5E), of which 22 were

upregulated and 50 were downregulated. Proteins related to tissue leakage and immunoglobulins were upregulated, while acute phase proteins, coagulation proteins, lipoproteins, and some immunoglobulins were downregulated. Overall, the variation in PC on hND-Tf-PNs offered nanoparticles the ability to decrease phagocytosis and clearance. Thus, nanoparticles can circulate in blood for extended periods, which increases the probability that they will reach the desired destination.

### 3.7. Qualitative analysis of PC derived from mice plasma *in vivo*

The same analysis was conducted for mice-derived PC *in vivo*. After classification according to their biological function, the

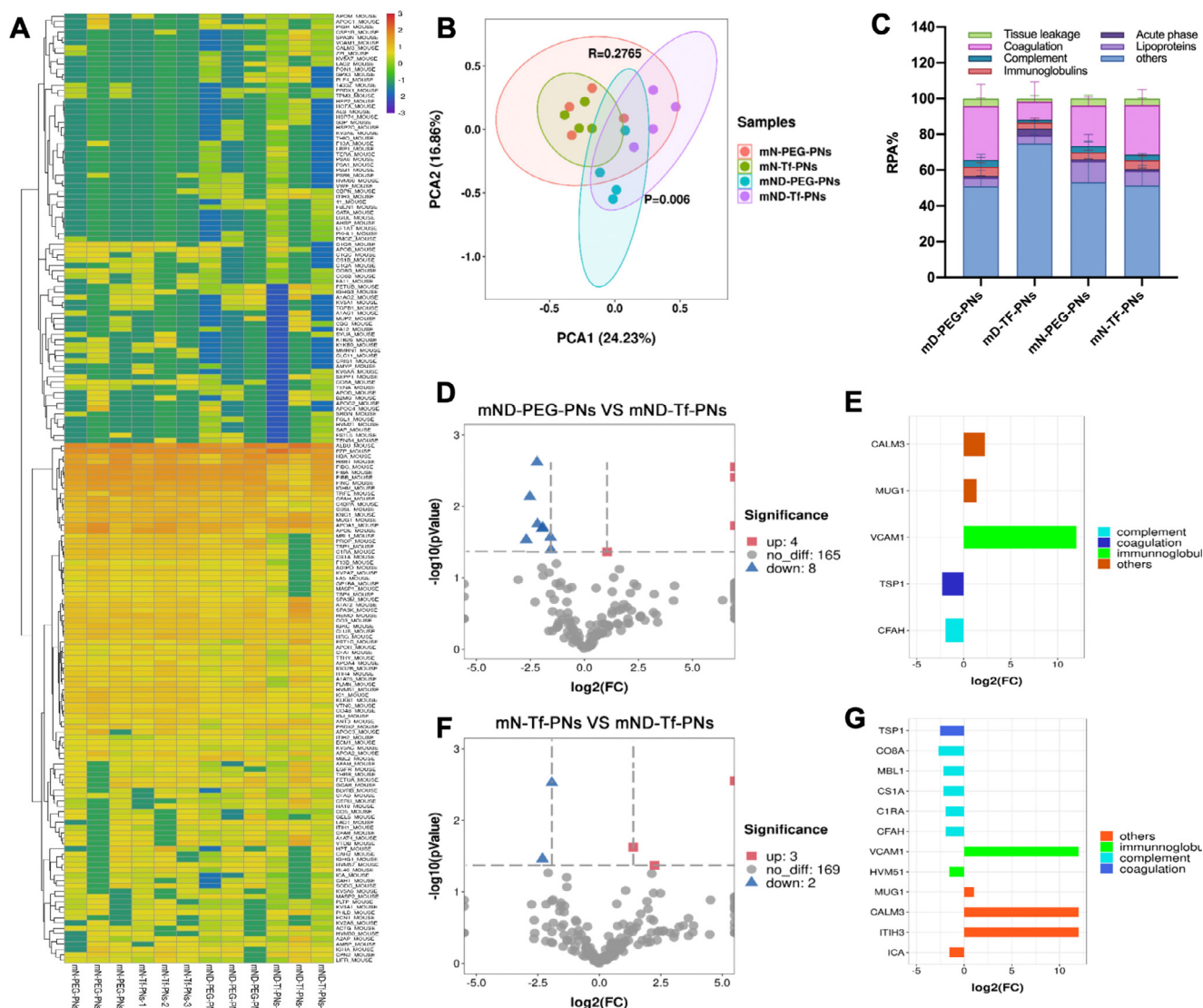


**Fig 6 – Qualitative analysis of PC derived from mice plasma in vivo. (A) Heat map of RPA% of PC derived from mice plasma in vivo. (B) Principal component analysis (PCA) of the corona proteins identified on PNs. (C) Bioinformatic classification of corona proteins. (D) Volcano plot of differential proteins between mND-Tf-PNs and mND-PEG-PNs. (E) Clustering of differential proteins between mND-Tf-PNs and mND-PEG-PNs. (F) Volcano plot of differential proteins between mND-Tf-PNs and mN-Tf-PNs. (G) Clustering of differential proteins between mND-Tf-PNs and mN-Tf-PNs.**

proteins’ RPA of coagulation, tissue leakage, and lipoproteins are diminished in the mND-Tf-PNs group. These differences may indicate that mND-Tf-PNs have a longer circulation time and less clearance (Fig. 6C). The volcano plot results show that there were 12 significant differential proteins in PC of the mND-Tf-PNs group, compared with that of mN-Tf-PN (Fig. 6F and 6G). Overall, the downregulated TSP1 (thrombospondin 1), immunoglobulins, coagulation proteins, and complements may suppress immune activation and prolong the circulation of PNs in the body. Conversely, the upregulated proteins may reduce the degradation of PNs and prolong the circulation of PNs. However, we observed significant differences in proteins and PC composition *in vivo* and *in vitro*, which may be due to species differences between humans and mice.

Based on the characteristics above, the composition of PC derived from different clinical states varied substantially, and this discrepancy seemed to lead to the *in vivo* behavior changes of nanoparticles.

#### 4. Conclusion

A systematic investigation was conducted to reveal the differences between PNs with PC derived from NSCLC comorbid with T2DM patients/model mice and NSCLC patients/model mice via *in vitro* and *in vivo* experiments. The Tf-modified PEGylated polystyrene nanoparticles increased cellular uptake via the Tf receptor-mediated pathway, but the

existence of PC significantly decreased the targeting ability of the Tf ligand. Moreover, the degree of influence varied with disease state. Tf-PNs with PC derived from NSCLC comorbid with T2DM accumulated more in cells and tumor tissue than those with NSCLC-derived PC.

Tf-PNs and PEG-PNs are hydrophilic nanoparticles; thus, they are more likely to absorb albumin, fibrinogen, and IgG. NSCLC comorbid with T2DM derived PCs contain more fibrin and polyproteins, which may help nanoparticles evade non-characteristic intake. In addition, fewer proteins, like complements, attached to nanoparticles could increase the circulation time in the body and increase the chances of reaching their target destination.

We conclude that comorbidity clinical status varied the composition of PC so to affect the bio-behavior of PNs and the Tf-PNs. Our results provide a new idea for improving the targeting ability of nanoparticles by precoating some proteins from plasma or biological environments. Furthermore, disease diagnostics could be improved by analyzing the PC of nanoparticles recovered from patients in the future. This work improves our understanding of how the disease state alters the formation of PC and how PC affects the behavior of nanoparticles in organisms. Additionally, the results provide a theoretical basis for the analysis and utilization of PC fingerprint maps for different diseases.

Future studies must investigate each different protein's function. In addition, only hard coronae were collected and analyzed due to methodological constraints. The result will be more accurate and authentic after a more advanced method is conducted to collect and detect soft coronae in real exposure scenarios.

## Conflicts of interest

The authors report no conflicts of interest. The authors alone are responsible for the content and writing of this article.

## Acknowledgements

The authors acknowledge the assistance of Tingting Li (Minister Science and Education) and thank the patients at People's Hospital of Xishuangbanna DAI autonomous prefecture for providing plasma samples. This work was supported by the Key Research and Development Program of Science and Technology Department of the Sichuan Province 111 Project (B18035). The author acknowledge the Letpub ([www.letpub.com](http://www.letpub.com)) for its linguistic assistance during the preparation of this manuscript and acknowledge Biorender ([www.biorender.com](http://www.biorender.com)) for its icon creating.

## REFERENCES

- [1] Cai R, Chen CY. The crown and the scepter: roles of the protein Corona in nanomedicine. *Adv Mater* 2019;31(45):e1805740.
- [2] Langer R. Drug delivery and targeting. *Nature* 1998;392(6679):5–10.
- [3] Belfiore L, Saunders DN, Ranson M, Thurecht KJ, Storm G, Vine KL. Towards clinical translation of ligand-functionalized liposomes in targeted cancer therapy: challenges and opportunities. *J Control Release* 2018;277:1–13.
- [4] Zhang H, Wu T, Yu W, Ruan S, He Q, Gao H. Ligand size and conformation affect the behavior of nanoparticles coated with *in vitro* and *in vivo* protein corona. *ACS Appl Mater Interfaces* 2018;10(10):9094–103.
- [5] Digiacoimo L, Pozzi D, Amenitsch H, Caracciolo G. Impact of the biomolecular corona on the structure of PEGylated liposomes. *Biomater Sci* 2017;5(9):1884–8.
- [6] Lesniak A, Fenaroli F, Monopoli MP, Åberg C, Dawson KA, Salvati A. Effects of the presence or absence of a protein corona on silica nanoparticle uptake and impact on cells. *ACS Nano* 2012;6(7):5845–57.
- [7] Lynch I, Salvati A, Dawson KA. Protein-nanoparticle interactions: what does the cell see? *Nat Nanotechnol* 2009;4(9):546–7.
- [8] Tenzer S, Docter D, Kuharev J, Musyanovych A, Fetz V, Hecht R, et al. Rapid formation of plasma protein corona critically affects nanoparticle pathophysiology. *Nature Nanotech* 2013;8(10):772–81.
- [9] Kreuter J. Nanoparticulate systems for brain delivery of drugs. *Adv Drug Deliv Rev* 2001;47(1):65–81.
- [10] Jiang Z, Guan J, Qian J, Zhan C. Peptide ligand-mediated targeted drug delivery of nanomedicines. *Biomater Sci* 2019;7(2):461–71.
- [11] Wang Y, Zhang H, Xiao W, Liu Y, Zhou Y, He X, et al. Unmasking CSF protein corona: effect on targeting capacity of nanoparticles. *J Control Release* 2021;333:352–61.
- [12] Salvati A, Pitek AS, Monopoli MP, Prapainop K, Bombelli FB, Hristov DR, et al. Transferrin-functionalized nanoparticles lose their targeting capabilities when a biomolecule corona adsorbs on the surface. *Nat Nanotechnol* 2013;8(2):137–43.
- [13] Monopoli MP, Åberg C, Salvati A, Dawson KA. Biomolecular coronas provide the biological identity of nanosized materials. *Nature Nanotech* 2012;7(12):779–86.
- [14] Papi M, Caputo D, Palmieri V, Coppola R, Palchetti S, Bugli F, et al. Clinically approved PEGylated nanoparticles are covered by a protein corona that boosts the uptake by cancer cells. *Nanoscale* 2017;9(29):10327–34.
- [15] Lacerda SHDP, Park JJ, Meuse C, Pristinski D, Becker ML, Karim A, et al. Interaction of gold nanoparticles with common human blood proteins. *ACS Nano* 2010;4(1):365–79.
- [16] Di Domenico M, Pozzi D, Palchetti S, Digiacoimo L, Iorio R, Astarita C, et al. Nanoparticle-biomolecular corona: a new approach for the early detection of non-small-cell lung cancer. *J Cell Physiol* 2019;234(6):9378–86.
- [17] Colapicchioni V, Tilio M, Digiacoimo L, Gambini V, Palchetti S, Marchini C, et al. Personalized liposome-protein corona in the blood of breast, gastric and pancreatic cancer patients. *Int J Biochem Cell Biol* 2016;75:180–7.
- [18] Kobos LM, Alqatani S, Ferreira CR, Aryal UK, Hedrick V, Sobreira TJP, et al. An integrative proteomic/lipidomic analysis of the gold nanoparticle biocorona in healthy and obese conditions. *Appl In Vitro Toxicol* 2019;5(3):150–66.
- [19] Lesniak A, Fenaroli F, Monopoli MP, Åberg C, Dawson KA, Salvati A. Effects of the presence or absence of a protein corona on silica nanoparticle uptake and impact on cells. *ACS Nano* 2012;6(7):5845–57.
- [20] Lesniak A, Salvati A, Santos-Martinez MJ, Radomski MW, Dawson KA, Åberg C. Nanoparticle adhesion to the cell membrane and its effect on nanoparticle uptake efficiency. *J Am Chem Soc* 2013;135(4):1438–44.
- [21] Sacchetti C, Motamedchaboki K, Magrini A, Palmieri G, Mattei M, Bernardini S, et al. Surface polyethylene glycol

- conformation influences the protein corona of polyethylene glycol-modified single-walled carbon nanotubes: potential implications on biological performance. *ACS Nano* 2013;7(3):1974–89.
- [22] Yu L, Xu M, Xu W, Xiao W, Jiang X, Wang L, et al. Enhanced cancer-targeted drug delivery using precoated nanoparticles. *Nano Lett* 2020;20(12):8903–11.
- [23] Nilsson J, Berglund A, Bergström S, Bergqvist M, Lambe M. The role of comorbidity in the management and prognosis in nonsmall cell lung cancer: a population-based study. *Acta Oncol* 2017;56(7):949–56.
- [24] Bi G, Yao G, Bian Y, Xue L, Zhang Y, Lu T, et al. The effect of diabetes mellitus on prognosis of patients with non-small-cell lung cancer: a systematic review and meta-analysis. *Ann Thorac Cardiovasc Surg* 2020;26(1):1–12.
- [25] Wang G, Li X, Xiong R, Wu H, Xu M, Xie M. Long-term survival analysis of patients with non-small cell lung cancer complicated with type 2 diabetes mellitus. *Thorac Cancer* 2020;11(5):1309–18.
- [26] Deng H, Zheng X, Zha P, Peng L, Huang K, Qiu X. Diabetes mellitus and survival of non-small cell lung cancer patients after surgery: a comprehensive systematic review and meta-analysis. *Thorac Cancer* 2019;10(3):571–8.
- [27] Yang X, Liu Y, Mani H, Olson J, Clawson G, Caruso C, et al. Biologic evaluation of diabetes and local recurrence in non-small cell lung cancer. *Pathol Oncol Res* 2017;23(1):73–7.
- [28] Hadjidemetriou M, McAdam S, Garner G, Thackeray C, Knight D, Smith D, et al. The human *in vivo* biomolecule corona onto PEGylated liposomes: a proof-of-concept clinical study. *Adv Mater* 2019;31(4):180335.
- [29] Zhang Z, Guan J, Jiang Z, Yang Y, Liu J, Hua W, et al. Brain-targeted drug delivery by manipulating protein corona functions. *Nat Commun* 2019;10(1):3561.
- [30] Holzapfel V, Musyanovych A, Landfester K, Lorenz M, Mailänder V. Preparation of fluorescent carboxyl and amino functionalized polystyrene particles by miniemulsion polymerization as markers for cells. *Chem Phys* 2005; 206(24): 2440–9.
- [31] Baribault H. Mouse models of type 2 diabetes mellitus in drug discovery. In: Proetz G, Wiles MV, editors. *Mouse models for drug discovery. methods in molecular biology*. New York: Humana Press; 2016. p. 153–75.
- [32] Szebeni J. Complement activation-related pseudoallergy: a new class of drug-induced acute immune toxicity. *Toxicology* 2005;216(2–3):106–21.
- [33] Pustulka SM, Ling K, Pish SL, Champion JA. Protein nanoparticle charge and hydrophobicity govern protein corona and macrophage uptake. *ACS Appl Mater Interfaces* 2020;12(43):48284–95.
- [34] Oh N, Park JH. Surface chemistry of gold nanoparticles mediates their exocytosis in macrophages. *ACS Nano* 2014;8(6):6232–41.
- [35] Wang Y, Zhang H, Xiao W, Liu Y, Zhou Y, He X, et al. Unmasking CSF protein corona: effect on targeting capacity of nanoparticles. *J Control Release* 2021;333:352–61.
- [36] Xiao W, Wang Y, Zhang H, Liu Y, Xie R, He X, et al. The protein corona hampers the transcytosis of transferrin-modified nanoparticles through blood–brain barrier and attenuates their targeting ability to brain tumor. *Biomaterials* 2021;274:120888.
- [37] Walkey CD, Chan WCW. Understanding and controlling the interaction of nanomaterials with proteins in a physiological environment. *Chem Soc Rev* 2012;41(7):2780–99.
- [38] Ni H, Denis CV, Subbarao S, Degen JL, Sato TN, Hynes RO, et al. Persistence of platelet thrombus formation in arterioles of mice lacking both von Willebrand factor and fibrinogen. *J Clin Invest* 2000;106(3):385–92.
- [39] Suh TT, Holmbäck K, Jensen NJ, Daugherty CC, Small K, Simon DI, et al. Resolution of spontaneous bleeding events but failure of pregnancy in fibrinogen-deficient mice. *Genes Dev* 1995;9(16):2020–33.
- [40] Riaz MA, Stammli A, Borgers M, Konrad L. Clusterin signals via ApoER2/VLDLR and induces meiosis of male germ cells. *Am J Transl Res* 2017;9(3):1266–76.
- [41] Lynch I, Dawson KA. Protein-nanoparticle interactions. *Nano Today* 2008;3(1):40–7.
- [42] Schöttler S, Becker G, Winzen S, Steinbach T, Mohr K, Landfester K, et al. Protein adsorption is required for stealth effect of poly(ethylene glycol)- and poly(phosphoester)-coated nanocarriers. *Nature Nanotech* 2016;11(4):372–7.
- [43] Thiele L, Diederichs JE, Reszka R, Merkle HP, Walter E. Competitive adsorption of serum proteins at microparticles affects phagocytosis by dendritic cells. *Biomaterials* 2003;24(8):1409–18.
- [44] Kukulj S, Jaganjac M, Boranic M, Krizanac S, Santic Z, Poljak-Blazi M. Altered iron metabolism, inflammation, transferrin receptors, and ferritin expression in non-small-cell lung cancer. *Med Oncol* 2010;27(2):268–77.
- [45] Basuli D, Tesfay L, Deng Z, Paul B, Yamamoto Y, Ning G, et al. Iron addiction: a novel therapeutic target in ovarian cancer. *Oncogene* 2017;36(29):4089–99.
- [46] Gu Z, Wang H, Xia J, Yang Y, Jin Z, Xu H, et al. Decreased ferroportin promotes myeloma cell growth and osteoclast differentiation. *Cancer Res* 2015;75(11):2211–21.
- [47] Xue D, Zhou CX, Shi YB, Lu H, He XZ. Decreased expression of ferroportin in prostate cancer. *Oncol Lett* 2015; 10(2): 913–6.